Contents lists available at ScienceDirect

Materials Science & Engineering A

Fatigue damage in coarse-grained lean duplex stainless steels

R. Strubbia *, S. Hereñú, M.C. Marinelli, I. Alvarez-Armas

Instituto de Física Rosario – CONICET, Universidad Nacional de Rosario, Argentina

ABSTRACT

The present investigation is focused on assessing the effect of a thermal treatment for grain coarsening on the low cycle fatigue damage evolution in two types of Lean Duplex Stainless Steels (LDSSs). The dislocation structure developed during cycling is observed by transmission electron microscopy (TEM). Additionally, a detailed analysis of short crack initiated and grown during low cycle fatigue (LCF) is performed by means of optical and scanning electron (SEM) microscopy in combination with automated electron back-scattered diffraction (EBSD) technique. Though in both coarse-grained LDSSs the short cracks nucleate in the ferrite phase, in each steels its origin is different. The embrittlement caused by the Cr_2N precipitation and the plastic activity sustained by each phase can explain this difference. The propagation behavior of the short cracks present two alternative growing mechanisms: the crack grows along a favorable slip plane with high Schmid Factor (SF) or the crack alternates between two slip systems. In both cases, the crack follows the path with the smallest tilt angle (β) at a grain boundary.

© 2016 Elsevier B.V. All rights reserved.

1. Introduction

The degradation of the material resulting from cyclic stress/strain called fatigue damage comprises several stages. The early stage of this process is the concentration of cyclic plastic strain formed during the dislocation structure evolution. Slip bands, inclusions, precipitates, grain boundaries and twin boundaries could exert this local plastic concentration. In these sites the first microcracks nucleates. The microcracks form, grow and/or coalesce generating a macrocrack which propagates up to the fracture of the material. The period of short crack initiation and growth determines in most cases the fatigue life of a specimen. The main feature for those short cracks is that their nucleation and propagation rate is strongly influenced by the microstructure. Particularly, in multiphase alloys there are a large number of parameters which can influence fatigue damage, such as chemical composition, microstructural morphology and the local plastic activity of each phase [1,2].

Duplex stainless steels (DSSs) are two-phase austenitic (γ)-ferritic (α) alloys with principal alloying elements chromium, nickel and molybdenum. Thanks to the attractive combination of mechanical properties and corrosion resistance, DSSs are widely used in different industries as; petrochemical, pulp and paper, chemical tankers and architecture. The fluctuating alloying element prices (especially nickel and molybdenum) during the last

decade has accelerated the development of more economic DSSs named Lean DSS (LDSSs). In LDSSs, the expensive nickel is partly substituted by nitrogen and manganese without degradation of corrosion and mechanical properties [3,4]. The usual manufacture process of DSSs, includes alternative steps of rolling and annealing, resulting in a lamellar microstructure of both phases with fine grains. The fatigue damage can be studied to its early stages by observation of the dislocation structure, by following the evolving surface relief and later by observing short crack nucleation and growth [5,6]. Therefore, in order to simplify the microcrack observation in DSSs during fatigue the grains are usually coarsened by a heat treatment of at 1250 °C followed by slow cooling to 1050 °C followed by a water-quenched [7–11]. This grain coarsening heat treatment (GCT) not only can change the morphology of the individual phases but also other microstructural modifications can take place. In this respect, it should be taken into account that precipitation of nitrides occurs after rapid cooling from high temperatures in ferritic steels, as in the ferritic phase of DSSs [12–14]. During this rapid cooling there is insufficient time for diffusion of nitrogen into austenite and the ferritic phase becomes supersaturated with nitrogen. Thus, intragranular chromium nitrides precipitate in ferrite with detrimental effects on material properties [13,14].

Additionally, it is also important to consider that depending on the microstructure and chemical composition of the austenitic phase of DSSs strain-induced martensitic transformation may occur [15,16]. Chiu et al. [17] suggest that the strain-induced martensitic transformation in metastable austenitic stainless steels

* Corresponding author.
E-mail address: strubbia@ifir-conicet.gov.ar (R. Strubbia).

have a beneficial effect on the fatigue resistance. The formation of strain-induced martensite in austenite of low stacking-fault energy (SFE) is closely related to shear bands, which are planar defects associated with the overlapping of stacking faults [18]. It is worth noting that the martensite transformation is enhanced by a lower SFE. In this sense, Jun and Choi [19] studied the correlation between the SFE and the austenite grain size in an Fe-Mn binary system. They showed that the SFE decreases rapidly with the increase of the austenite grain size in the range of $13 - 35$ μm, over which SFE comes in a saturation region up to 185 μm. Recently, Saeed-Akbari et al. [20] evalued the grain size dependency of SFE in High-Manganese Steels. They found that SFE decreases as the grain size increases for austenite grain size in the range of $5 - 50$ μm.

Thus, the results of the fatigue damage in GCT-DSSs should be carefully analyzed before performing a direct extrapolation to those expected in as-received DSSs. Therefore, this work intends to highlight the influence of GCT on the fatigue damage of two different LDSSs.

2. Material and experimental procedure

2.1. Material

The investigated materials were two LDSSs, LDX 2101 (UNS S32101) and AL 2003 (UNS S S32003). Table 1 gives the chemical composition in weight percent of both LDSSs. These LDSSs were selected taken into account their different Ni contents. LDSS AL 2003 (UNS S32003) has a chemical composition similar to the standard SAF 2205 while LDX 2101 (UNS S32101) is more representative of LDSSs. These steels were received in longitudinally welded stainless steel pipes. The manufacturing process of the pipes includes a hot rolled stage and a subsequent welding of the tube. A thermal treatment at 1050 °C followed by a water quench was finally carried out to the tube. The steels supplied after this industrial process will be hereinafter designated as as-received (AR). In this condition [11,21], a lamellar structure of austenite and ferrite is distinguished in the rolling direction with no evidence of any additional secondary phases. A coarse grain structure of DSSs facilitates microcracks observation, so the AR materials were solution annealed 2 h at 1250 °C followed by slow cooling to 1050 °C (to regain identical fractions of austenite and ferrite) and subsequent water quenching. LDSSs with coarse grains will be referred as coarse grain thermal treated LDSSs (GCT – LDSSs).

2.2. Experimental procedure

Metallographic preparation of specimens included a standard mechanical grinding procedure and a two-step electrolytic etching, method documented to be successful for providing indirect evidence for the presence of nitrides and revealing the microstructure of the samples [13]. Nevertheless, grain boundaries are slightly visible using this etching procedure. Therefore, SEM electron backscattered diffraction (SEM-EBSD) technique was used as a quantitative characterization tool [22]. The use of this technique enabled us to determine the average grain size and volume fraction of each phase whereas the microhardness of both phases of

each LDSS was also measured (Table 2). The Vickers indentations were performed with a load of 245.2 mN during 10 s For each sample a minimum of 10 measures were carried out. With these results thereafter, the corresponding medium value with its standard deviation was calculated.

From slabs taken parallel to the axis of the pipe, flat specimens were prepared by electro erosion with a 20 mm gauge length and a section of 30 mm². In order to obtain a smooth surface for the fatigue tests, all the specimens were initially ground and polished with sequentially finer grits. These specimens were used to obtain the cyclic stress–strain curves under fully reversed total strain control, applying a triangular waveform at a constant total strain rate of $\dot{\varepsilon} = 2 \times 10^{-3} \, \mathrm{s}^{-1}$, with total strain range of $\Delta\varepsilon_t = 0.6\%$. This total strain value corresponds to a plastic strain range, measured from the hysteresis loop at midlife to fracture, of approximately $\Delta\varepsilon_p = 0.2\%$. In order to observe the damage evolution during LCF tests, additional cyclic tests were conducted at room temperature under fully reversed plastic strain control, with a plastic strain range of $\Delta\varepsilon_p = 0.2\%$. Under these conditions, tests were repeated five times so as to detect in each phase the surface relief associated with initial slip lines and the subsequent microcrack nucleation and growth. Specimens for these tests were further electrolytic-polished; using a solution of 10% perchloric acid in ethanol as electrolyte. This surface preparation allows the observation of the structure during tests and the acquisition of good quality electron back-scattered diffraction patterns (EBSD). Surface damage observations of a central sector of the specimens were performed by in situ microscopy before and during the LCF test using an optical system composed of a CCD camera JAI mod. CM-140MCL with a 50 × objective, focal length of 13 mm, depth of field of ± 1 μm and a 12 × ultra zoom device mounted on the fatigue test machine. After LCF tests a Scanning Electron Microscope (SEM) equipped with EBSD detector was used to determine the slip systems, their Schmid Factor (SF) and their angles relative to the tensile axis. On the other hand, the angles between the surface slip markings and the loading axis were measured. The comparison of these angles with the calculated ones permits to identify the activate slip systems and theirs corresponding SFs.

In order to analyze the dislocation structure before and after fatigue thin foils were observed by TEM operating at 100 kV.

3. Results and discussion

Table 2 summarizes the average grain size, volume fraction and hardness of each phase in GCT-LDX 2101 and GCT-AL 2003. Fig. 1 shows the microstructure of both LDSSs after the GCT. Whereas the microstructure of the AR LDSSs have been characterized by lamellar phases highly elongated in the rolling direction with fine grains [11,21], an isotropic microstructure with a considerable increase of the grain size in both phases is produced by GCT. This figure also shows small etching pits in the ferrite phase of both steels, corresponding to Cr_2N. During cooling from high temperatures, as occurs in GCT, the solubility of nitrogen is much higher in austenite than in ferrite. Therefore, if the cooling rate is high enough to prevent diffusion of nitrogen into austenite, the ferrite gets supersaturated with nitrogen and chromium nitrides are then formed [12]. In this sense, as it is seen in Fig. 1, the nitrogen neighbour to the phase boundaries has had time to diffuse into the austenite avoiding the precipitation of Cr_2N. In LDSSs, nickel is partially replaced by nitrogen as an austenite stabilizer. However, a high concentration of manganese is also added to ensure adequate nitrogen solubility [23]. A higher density of chromium nitrides precipitate in the ferrite phase of GCT-AL2003 than in GCT-LDX 2101, consistent with the lower solubility of nitrogen in GCT-AL2003. This result agrees with the microhardness

Table 1
Chemical composition of LDSS AL 2003 and LDX 2101 in weight percent (wt%).

LDSS	C	Si	Mn	P	S	Ni	Cr	Mo	Cu	N
AL 2003	0.021	0.22	1.73	0.024	–	3.8	22	1.8	–	0.18
LDX 2101	0.026	0.63	4.9	0.021	0.001	1.53	21.53	0.28	0.33	0.22

Table 2
Grain size, volume fraction of phases and Vickers hardness of each phase in GCT- LDSSs.

Material	Phase	Average diameter (μm)	Standard deviation (μm)	Standard error of the mean (μm)	Volume fraction of phases	Vickers hardness (HV)
GCT-	Ferrita	10	20	2	0.45	270 ± 20
AL2003	Austenita	20	20	2	0.55	270 ± 20
GCT-	Ferrita	20	20	2	0.35	190 ± 20
LDX2101	Austenita	22	20	1	0.65	210 ± 10

reported in Table 2; being higher in GCT-AL 2003 than GCT-LDX 2101. The microscopic features of these precipitates in GCT- LDSSs were examined by transmission electron microscopy. Fig. 2 shows the characteristic needle shaped morphology of chromium nitrides [12–14].

Figs. 3 and 4 show the characteristic dislocation microstructure of both phases of GCT-AL 2003 and GCT-LDX 2101, respectively. It is interesting to note from Fig. 3(a) and Fig. 4(a) that a considerable dislocation density remains in the ferrite phase of both LDSSs after GCT [11,21]. As regards the austenite phase, several aspects may be pointed out. Whereas in GCT-AL 2003, no evidence of substructural changes are found (Fig. 3(b)) compared with those observed in AR-AL 2003 [21], a higher density of Shockley partial dislocations with wider stacking fault region is developed in GCT-LDX 2101 (Fig. 4(b)), than in AR-LDX 2101 [11].

Fig. 5 shows the cyclic hardening-softening responses at $\Delta\varepsilon_t=0.6\%$ of CGT-AL 2003 and CGT-LDX 2101 in comparison with the reported results in AR conditions [24]. Regardless of the thermal condition, AR or GCT, the general cyclic behavior of both LDSSs is characterized by an initial small cyclic hardening followed by a cyclic softening stage that sets in for most of the fatigue life. From this figure it is evident, in both thermal conditions (AR and GCT), a more pronounced cyclic softening of LDX 2101 than AL 2003.

In order to correlate the mechanical behavior with the dislocation structure of fatigued specimens, thin foils were prepared from specimens cycled up to failure. Referring to the ferritic phase of GCT-AL 2003, (Fig. 6(a)), no noticeable evolution of dislocation structure can be distinguished during cycling (Fig. 3(a)). On the other hand, during cycling in the ferrite phase of GCT- LDX 2101 the dislocation structure has evolved to loop patches (Fig. 6(b)). When analyzing the substructure developed within the austenite grains in both GCT-LDSSs planar arrays of dislocations, usually with more than one active slip system are found, Fig. 7(a) and (b). Furthermore, particularly in GCT- LDX 2101 a higher density of stacking faults with a large amount of intense deformation bands are formed during cycling (Fig. 7(b) and (c)). It is worthwhile to
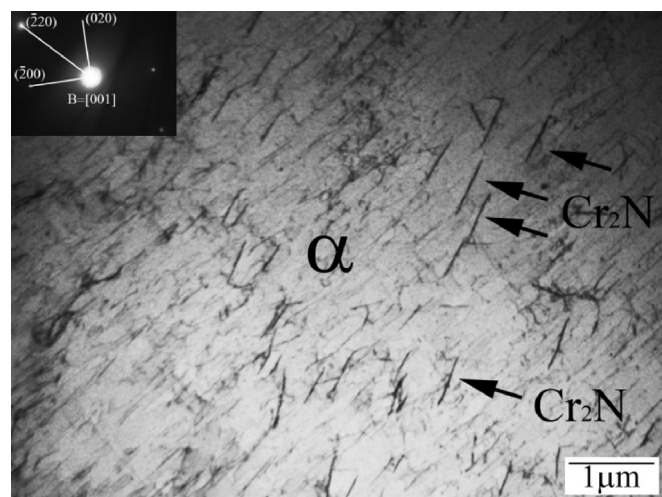
Fig. 2. Bright-field TEM image of needle shaped chromium nitrides Cr_2N within ferritic grains (B=[001]).

remark that in this steel needles of strain-induced α′ martensite has also been observed (Fig. 7(d)). Other authors [15,25] also reported the formation of strain-induced α′ martensite in LDSS under different deformation processes. Olson and Cohen [26] suggest that plastic deformation forms energetically favorable sites which promotes austenite transformation to α′ martensite. In this sense, some of these sites are intersections of shear bands, overlapping stacking faults, ε-martensite and mechanical twinning. Moreover, strain-induced ε-martensite needles can form if the stacking faults alternate "properly" in close parallel planes [27]. Depending on the stacking fault energy, the formation of α′ martensite can result directly from the austenite or from hexagonal ε−martensite. Moreover, wider stacking faults are observed in materials with lower SFE [19,20]. In this sense, the microstructural comparison of the austenite in AR-LDX 2101 and GCT- LDX 2101 suggests that the grain coarsening treatment decrease the SFE in the GCT-LDSS. It
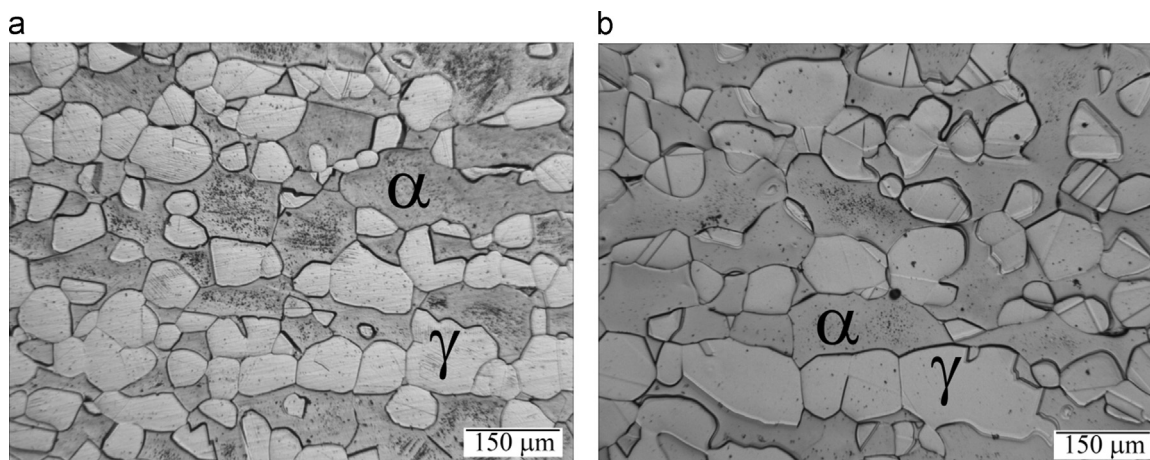
Fig. 1. Optical micrograph of (a) GCT-AL 2003 and (b) GCT-LDX 2101.

a

b
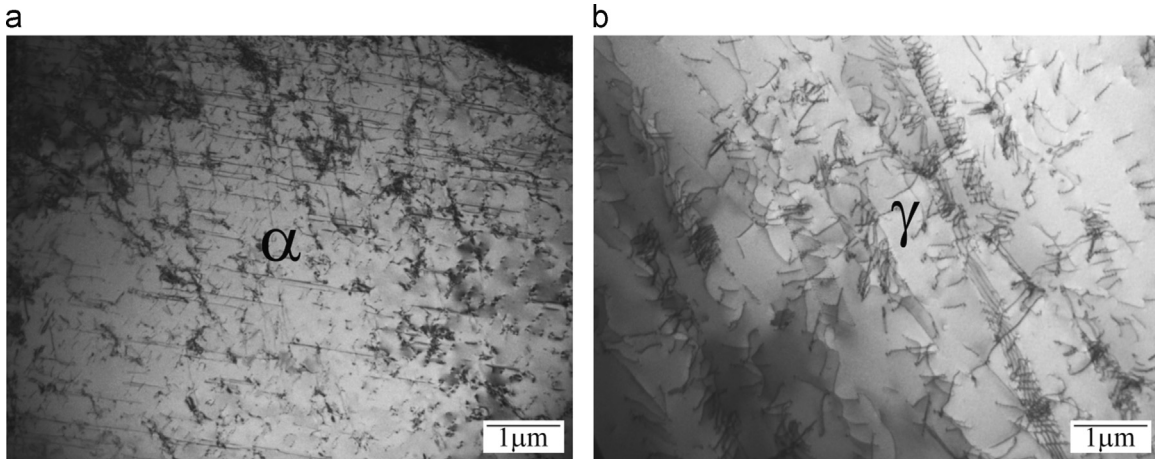
Fig. 3. Bright-field TEM images of AL 2003-GCT (a) ferrite (B=[011]) and (b) austenite (B=[$\bar{1}$14]).

a

b
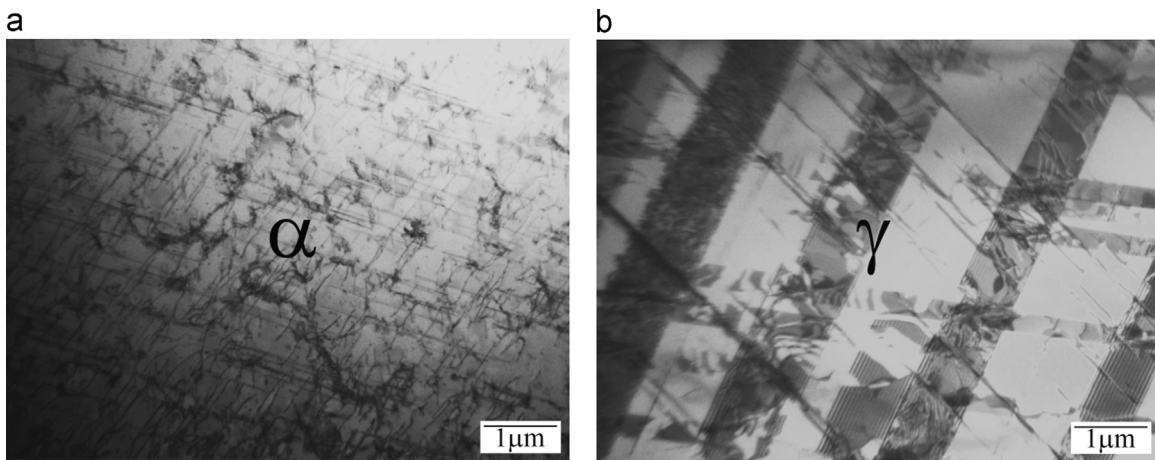
Fig. 4. Bright-field TEM images of GCT-LDX 2101 (a) ferrite (B=[$\bar{1}$13]) and (b) austenite (B=[011]).
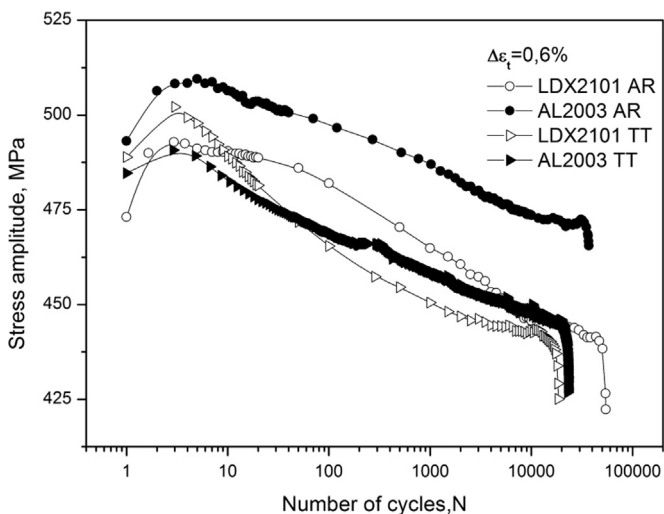
Fig. 5. Cyclic response of GCT-AL 2003 and GCT-LDX 2101 in comparison with AR conditions.

follows, therefore, that the austenite phase of CGT-LDX 2101 is more prone to transform into martensite than AR-LDX 2101. Although austenite-martensite mixture has been considered as a soft austenitic matrix composite with a distribution of hard martensite [28,29], in GCT-LDX 2101 it seems that the presence of martensite does not affect significantly the cyclic behavior (Fig. 5). This could

be due to the small amount of martensite found in this steel. In this sense, Hamada et al. [30] reported that a low content of strain-induced martensite does not produce a discernible influence on the cyclic behavior of austenitic steel 301LN. On the other hand, in GCT-AL 2003 as a result of its larger austenite grain size compared with those of the ferrite and the similar hardness of the phases (Table 2), the austenite phase supports most of the applied strain, Fig. 6(a) and Fig. 7(a). Conversely, in the GCT-LDX 2101 both phases have similar hardness and grain size (Table 2), so the applied strain is nearly equally distributed between the two phases, Fig. 6(b) and Fig. 7(b), (c) and (d). Nonetheless, in spite of the higher strain withstood by the austenite grains in GCT-AL 2003 than those in GCT-LDX 2101, the martensitic transformation was no detected in GCT-AL 2003. This can be rationalized by comparing the width of the stacking faults in GCT-AL 2003 and in GCT-LDX 2101 that gives evidence of lower SFE in the latter steel. Therefore, the austenite phase of LDX 2101 has a higher chance of transformation into martensite than the same phase of AL 2003.

As regards the cyclic softening displayed by the present LDSSs (Fig. 5), some aspects should be considered. It is well-known that nitrogen in solid solution in the austenite phase promotes the development of planar arrays of dislocations which enhances cyclic softening [31]. This fact can explain the cyclic softening observed in both GCT LDSSs. Moreover, the cyclic strain accommodation sustained by both phases of GCT-LDX 2101 could explain its higher cyclic softening respect to GCT-AL 2003.

The in situ observation of GCT-LDSSs specimens subject to LCF tests reveals that the first slip markings appear almost
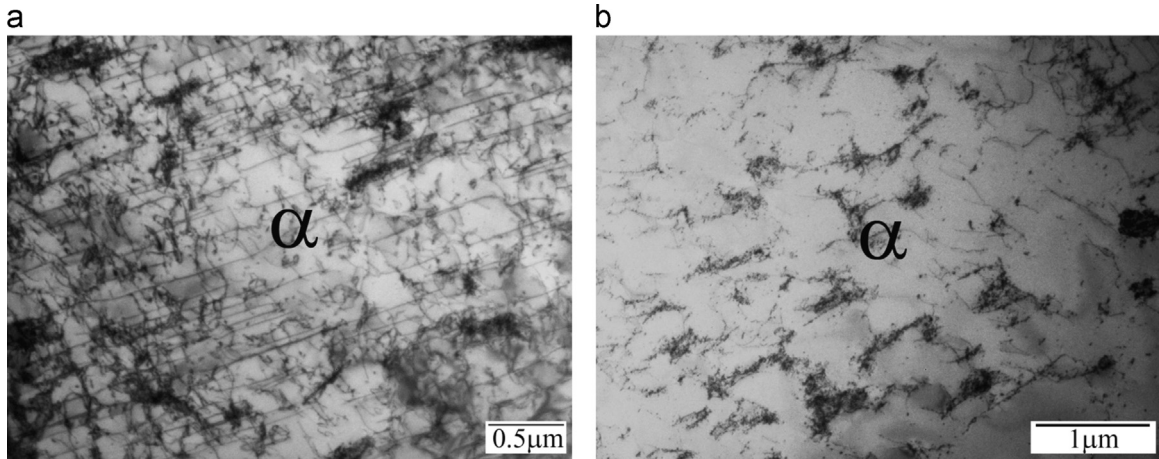
Fig. 6. Bright-field TEM images of ferrite phase of specimens subject to LCF at $\Delta\varepsilon_t=0.6\%$ to failure (a) GCT-AL 2003 (B=[011]) (b) GCT-LDX 2101(B=[$\bar{1}$13]).

simultaneously in both phases, Fig. 8(a) and Fig. 9(a). As cycling proceeds, while in GCT-AL 2003 the intensification of slip marking occurs mainly in the austenitic phase (Fig. 8(b)) in GCT-LDX 2101 takes place in the ferrite phase, Fig. 9(b). Nevertheless, in both GCT-LDSS microcracks nucleate in ferrite (Fig. 8(c) and Fig. 9(c)). The origin of this short crack nucleation is different in each case. According to a previous study in GCT-AL 2003, microcracks nucleate in the ferrite as result of the embrittlement caused by the Cr_2N precipitation [32]. The preceding fatigue damage evolution is corroborated in the present work (Fig. 8). In GCT-LDX 2101, in

addition to the detrimental effect of Cr_2N precipitation, the stronger plastic activity in the ferritic phase in comparison with that developed in austenite should be considered. In both AR-LDSS, cracks nucleate along extrusions in the ferrite phase as a result of the larger plastic activity found in this phase [11,21,24]. Thus, the differences of fatigue damage between AR and GCT-LDSSs can be ascribed not only to strain partition changes in each phase but also to the detrimental chromium nitrides precipitation caused by the grain coarsening treatment. Therefore, the GCT has a strong influence on the fatigue damage of LDSSs. Thus, care should
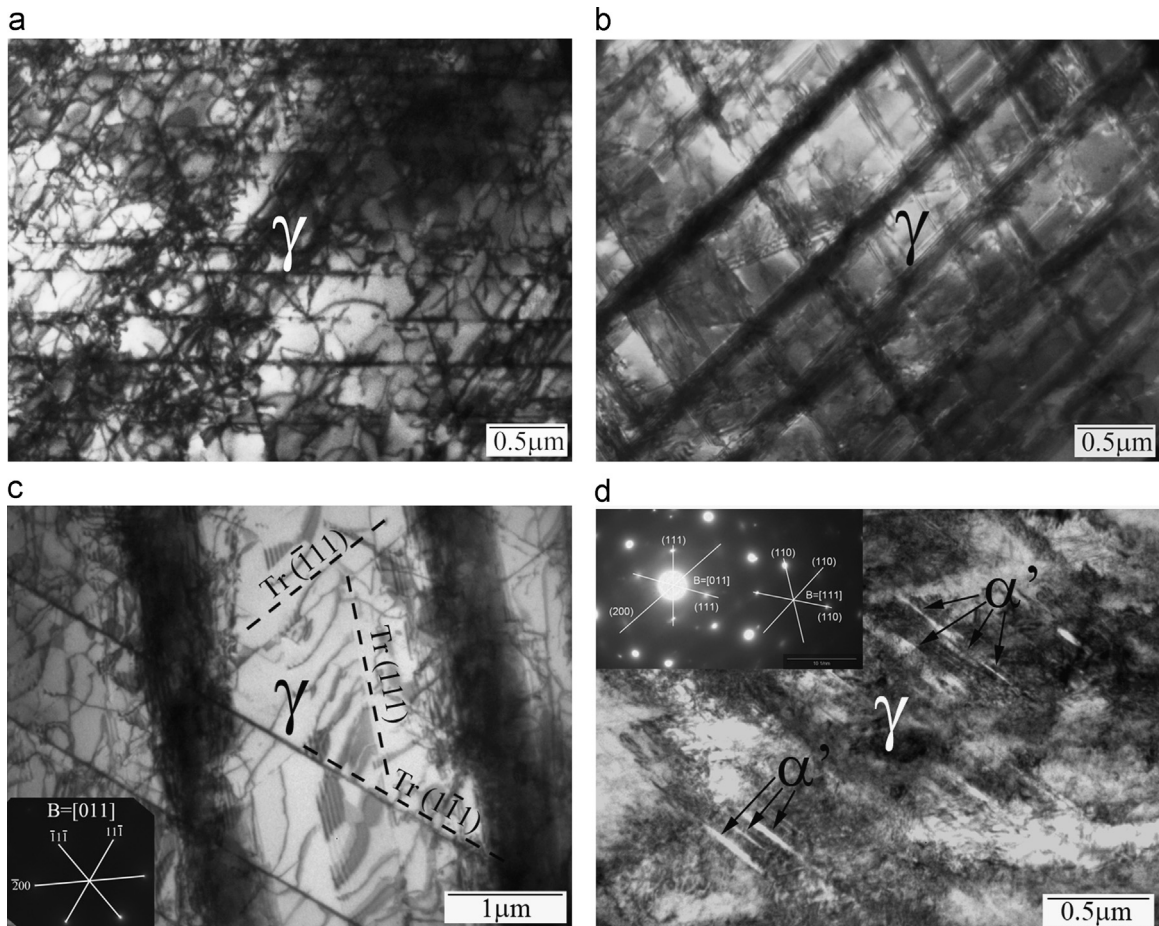
Fig. 7. Bright-field TEM images of austenitic phase of specimens subject to LCF at $\Delta\varepsilon_t=0.6\%$ up to failure (a) GCT- AL 2003 (B=[011]), (b) (B=[011]), (c) (B=[011]) and (d) GCT-LDX 2101(B=[013]).
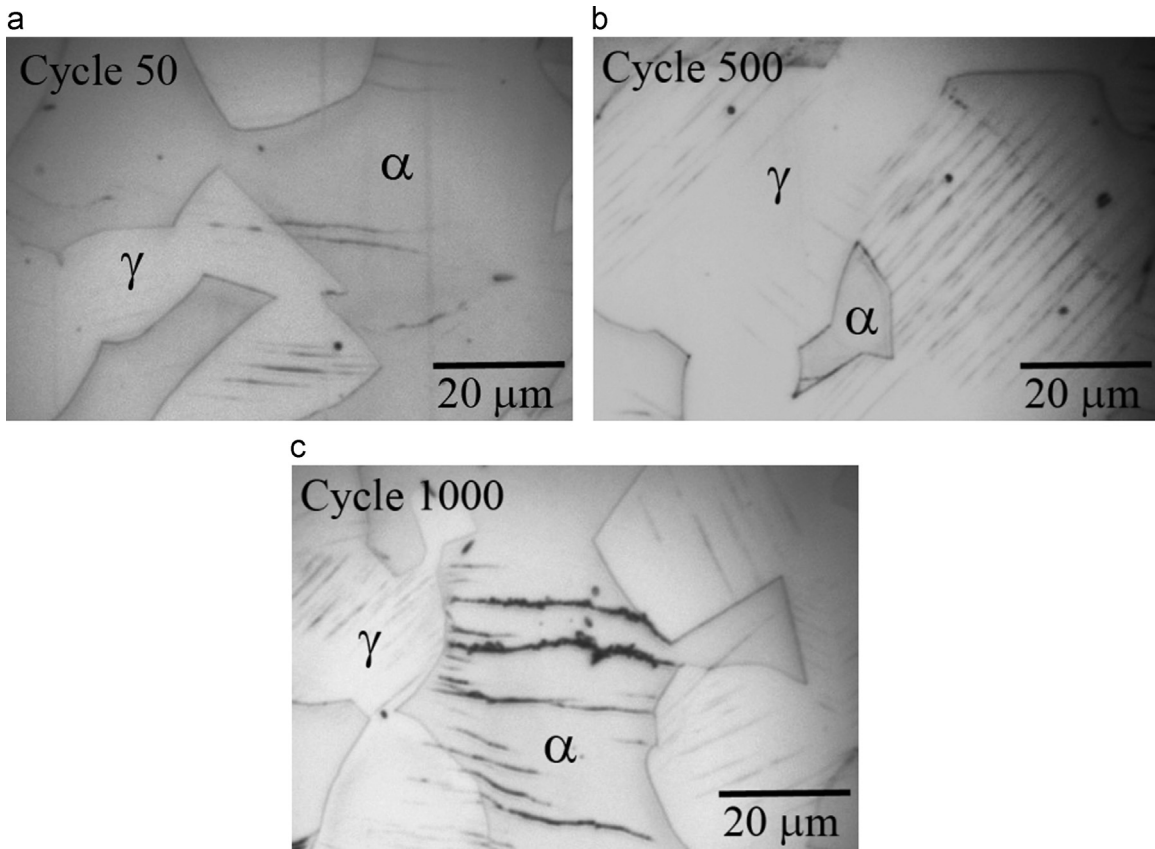
Fig. 8. Surface damage evolution of GCT-AL2003 subject to LCF a) cycle 50, b) cycle 500 and c) cycle 1000.
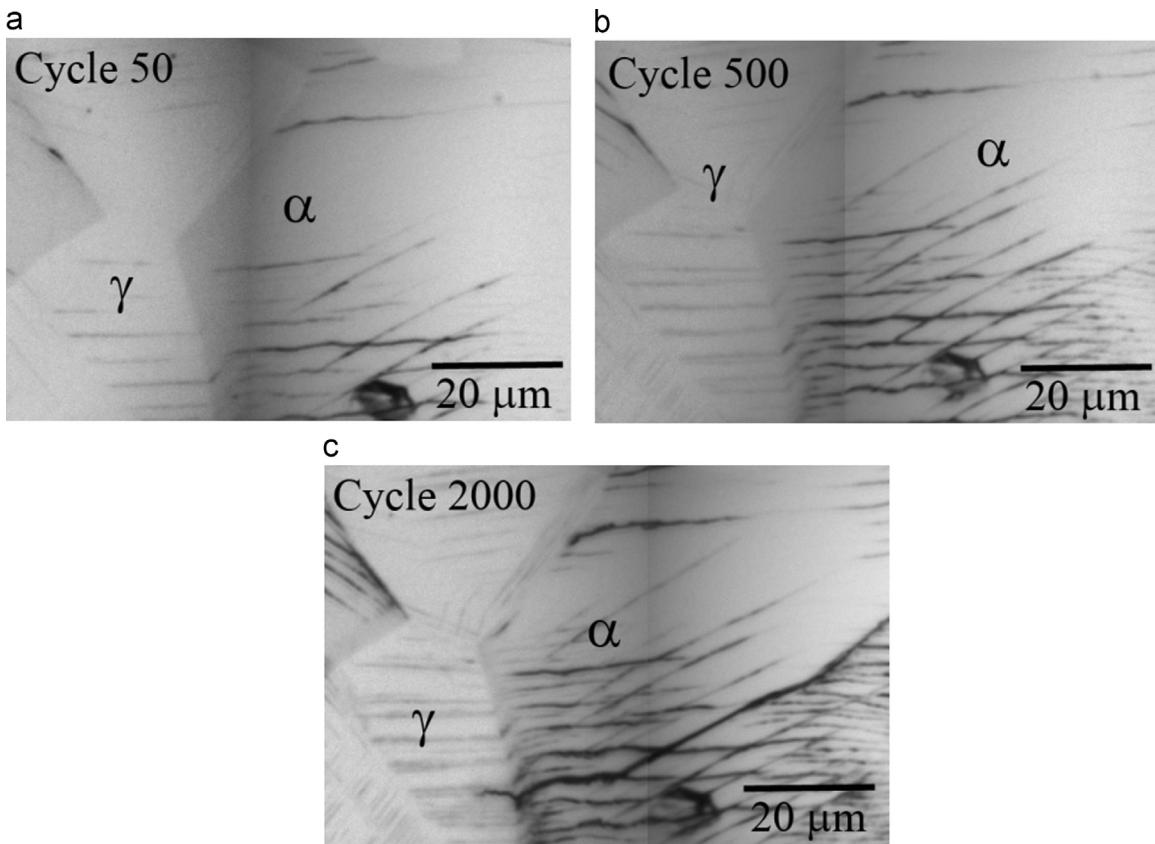
Fig. 9. Surface damage evolution of GCT-LDX 2101 subject to LCF a) cycle 50, b) cycle 500 and c) cycle 2000.
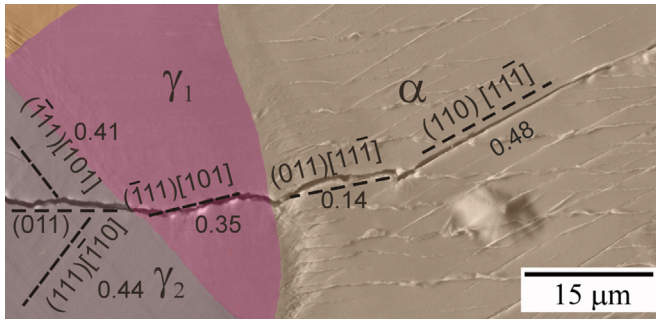
Fig. 10. Analysis of short crack path, slip systems and SF, in GCT-LDX 2101.

Table 3
Crack-plane deflection at grain boundaries.

Crack-plane deflection at grain boundaries							
$\alpha \to \gamma_1$				$\gamma_1 \to \gamma_2$			
Crack-plane in α grain	Possible slip planes in γ_1	Twist (α)	Tilt (β)	Crack-plane in γ_1 grain	Possible slip planes in γ_2	Twist (α)	Tilt (β)
(0 1 1)	(1 1 $\bar{1}$)	18	13	($\bar{1}$ 1 1)	(1 1 $\bar{1}$)	11	44
	($\bar{1}$ 1 1)	38	10		($\bar{1}$ 1 1)	21	53
	(1 $\bar{1}$ 1)	57	65		(1 $\bar{1}$ 1)	31	51
	(1 1 1)	52	85		(1 1 1)	72	87

be taken in the extrapolation of the results obtained for GCT-LDSSs to those expected in AR-LDSSs.

Recent studies [11,21,33,34] dealing with the propagation behavior of short cracks have found that crack can present two alternative growing mechanisms, stage I or stage II. In Stage I, the crack grows along a favorable slip plane with high Schmid Factor (SF), while in stage II the crack alternates between two slip systems. Moreover, according to Zhai et al. [35], the twist (α) and tilt (β) angles of the crack-plane deflection at a grain boundary are the key factors that control the path and growth rate of a short crack. The smaller the twist (α) and the tilt (β) angles the lower the resistance to microcrack propagation. Thereby, to study the microcrack propagation, SEM observations in combination with EBSD technique were used in LDSSs. A previous study [32] analyzed the microcrack path in LDSS GCT-AL 2003. In the present work a detailed analysis of crack propagation in the GCT-LDX 2101 is performed. In this respect, a crack nucleated within the ferrite phase initially grows along a favorable slip plane with high Schmid Factor (SF) (stage I) and as it reaches an austenitic grain can grow by stage I or stage II, Fig. 10. According to Marinelli et al. [36] when α and β angles between two neighbouring grains are small, the flow of plasticity between grains is enhanced. Table 3 presents the α and β angles between the crack plane and the slip planes of neighbouring grains (Fig. 10). It is worth noting that in γ_1 the crack propagates along a slip system with the smallest β angle, but not necessarily with the smallest α angle. In γ_2 grain the crack resumes growing in stage II on lattice planes of {1 1 0} type. These results can be explained considering that the crack grows along a path that minimises the β angle. In this case the β angle between plane in γ_1 and in of γ_2 is smaller (17°) than those displayed in Table 3. This result agrees with that reported by Marinelli et al. [32] in GCT-AL 2003. It is important to remark that AR [11,21] and GCT-LDSS present similar trends with respect to short crack propagation mechanisms.

4. Conclusions

The grain coarsening treatment (GCT), usually performed to analyze the fatigue damage in AR-DSSs, produces microstructural changes that should be taken into account to avoid wrong extrapolations.

In AR-LDSSs the cyclic plastic activity is mainly sustained by the ferrite phase. On the other hand, in GCT-AL 2003 the austenite phase supports most of the applied strain while in the GCT-LDX 2101 the plastic deformation is bore by both phases. Also, a small amount of strain-induced martensite is observed in the austenite phase of GCT-LDX 2101, not causing a discernible effect on fatigue damage.

As in AR-LDSS, in both GCT-LDSSs cracks nucleate in the ferrite phase. However, in GCT-AL 2003 Cr_2N precipitation is the main reason for this nucleation while in GCT-LDX 2101 the higher plastic activity in the ferritic phase in comparison with that developed in austenite should be also added to the detrimental effect of Cr_2N precipitation. As regard the short crack propagation the GCT does not change the mechanism already observed in the AR-LDSS.

References

[1] J. Stolarz, J. Foct, Specific features of two phase alloys response to cyclic deformation, Mater. Sci. Eng. A 319–321 (2001) 501–505.
[2] J. Polak, P. Zezulka, Short crack growth and fatigue life in austenitic-ferritic duplex stainless steel, Fatigue Fract. Eng. Mater. Struct. 28 (2005) 923–935.
[3] Duplex Stainless Steels, (Eds.) I. Alvarez-Armas, S. Degallaix-Moreuil, ISTE Ltd. and John Wiley & Sons Inc., 2009.
[4] A. Kumar, Development and Characterization of Nickel Free Duplex Stainless Steel, Thapar University, 2008, http://dspace.thapar.edu:8080/dspace/bit stream/10266/555/3/T555.pdf.
[5] S. Suresh, Fatigue of Materials, 2nd ed., Cambridge University Press, UK, 1998.
[6] J. Polak, Cyclic deformation, crack initiation and low cycle fatigue, in: I. Milne, R.O. Ritchie, B. Karihaloo (Eds.), Comprehensive Structural Integrity, vol. 4, Elsevier, Amsterdam, 2003, pp. 1–39.
[7] M. Scharnweber, W. Tirschler, C.-G. Oertel, W. Skrotzki, Mechanisms of short crack propagation in austenitic–ferritic duplex steel, Mater. Sci. Eng.: A 595 (2014) 269–283.
[8] M. Scharnweber, W. Tirschler, C.-G. Oertel, W. Skrotzki, Initiation and propagation of short cracks in austenitic–ferritic duplex steel, Mater. Sci. Eng.: A 583 (2013) 52–60.
[9] U. Krupp, A. Giertler, M. Söker, H. Fu, B. Dönges, H.-J. Christ, A. Hüsecken, U. Pietsch, C.-P. Fritzen, W. Ludwige, The behavior of short fatigue cracks during very high cycle (VHCF) fatigue of duplex stainless steel, Eng. Fract. Mech. 145 (2015) 197–209.
[10] H. Knobbe, P. Starke, S. Hereñú, H.-J. Christ, D. Eifler, Cyclic deformation behaviour, microstructural evolution and fatigue life of duplex steel AISI 329 LN, Int. J. Fatigue 80 (2015) 81–89.
[11] R. Strubbia, S. Hereñú, I. Alvarez-Armas, U. Krupp, Short fatigue cracks nucleation and growth in lean duplex stainless steel LDX 2101, Mater. Sci. Eng.: A 615 (2014) 169–174.
[12] A. Säfsten, Quantitative Phase Analysis of Duplex Stainless Steels as a Function of Heat Treatment, Luleå University of Technology, Sweden, 2009, http://epubl.ltu.se/1402-1617/2009/129/index-en.html.
[13] T.H. Iversen, Intragranular Chromium Nitride Precipitates in Duplex and Superduplex Stainless Steel, Norwegian University of Science and Technology, Norway, 2012, http://hdl.handle.net/11250/249085.
[14] S. Hereñú, M.G. Moscato, I. Alvarez-Armas, a F. Armas, Cyclic behavior of a superferritic stainless steel at room and intermediate temperatures, Int. J. Fatigue 65 (2014) 71–77.
[15] C. Herrera, D. Ponge, D. Raabe, Design of a novel Mn-based 1 GPa duplex stainless TRIP steel with 60% ductility by a reduction of austenite stability, Acta

Mater. 59 (2011) 4653–4664.

[16] S. Baldo, Innovative Steels for Structural and Corrosion Resistance Applications, Università degli Dtudi DI Padova, Italy, 2010, http://paduaresearch.cab.unipd.it/3398/1/Baldo.pdf.

[17] P.K. Chiu, K.L. Weng, S.H. Wang, J.R. Yang, Y.S. Huang, J. Fang, Low-cycle fatigue-induced martensitic transformation in SAF 2205 duplex stainless steel, Mater. Sci. Eng. A 398 (2005) 349–359.

[18] K.H. Lo, C.H. Shek, J.K.L. Lai, Recent developments in stainless steels, Mater. Sci. Eng.: R R65 (2009) 39–104.

[19] J.-H. Jun, C.-S. Choi, Variation of stacking fault energy with austenite grain size and its effect on the M_S temperature of $\gamma \rightarrow m$ martensitic transformation in Fe – Mn alloy, Mater. Sci. Eng. A 257 (1998) 353–356.

[20] A. Saeed-Akbari, J. Imlau, U. Prahl, W. Bleck, Derivation and variation in composition-dependent stacking fault energy maps based on subregular solution model in high-manganese steels, Metall. Mater. Trans. A 40 (2009) 3076–3090.

[21] R. Strubbia, S. Hereñú, A. Giertler, I. Alvarez-Armas, U. Krupp, Experimental characterization of short crack nucleation and growth during cycling in lean duplex stainless steels, Int. J. Fatigue 65 (2014) 58–63.

[22] N. Gao, S.C. Wang, H.S. Ubhi, M.J. Starink, A comparison of grain size determination by light microscopy and EBSD analysis, J. Mater. Sci. Lett. 40 (2005) 4971–4974.

[23] J.Y. Choi, J.H. Ji, S.W. Hwang, K.-T. Park, TRIP aided deformation of a near-Ni-free, Mn–N bearing duplex stainless steel, Mater. Sci. Eng. A 535 (2012) 32–39.

[24] R. Strubbia, S. Hereñú, M.C. Marinelli, I. Alvarez-Armas, Short crack nucleation and growth in lean duplex stainless steels fatigued at room temperature, Int. J. Fatigue 41 (2012) 90–94.

[25] I. Calliari, M. Dabalà, E. Ramous, New lean duplex stainless steels for structural applications, Mater. Sci. Forum 604–605 (2009) 419–426, http://dx.doi.org/10.4028/www.scientific.net/MSF.604-605.419.

[26] G.B. Olson, M. Cohen, A mechanism for the strain-induced nucleation of martensitic transformations, J. Less-Common Met. 28 (1972) 107–118.

[27] S. Ueda, H. Fujita, F.C.C. Strain-Induced, (γ)-HCP(ε) phase transformation and active slip systems, Trans. JIM 18 (1977) 169–177, https://www.jstage.jst.go.jp/article/matertrans1960/18/3/18_3_169/_article.

[28] P.L. Mangonon, G. Thomas, Structure and properties of thermal-mechanically treated 304 stainless steel, Metall. Trans. B 1 (6) (1970) 1587–1594.

[29] I. Tamura, Deformation-induced martensitic transformation and transformation-induced plasticity in steels, Met. Sci. 16 (1982) 245–253.

[30] A.S. Hamada, L.P. Karjalainen, P.K.C.V. Surya, R.D.K. Misra, Fatigue behavior of ultrafine-grained and coarse-grained Cr–Ni austenitic stainless steels, Mater. Sci. Eng.: A 528 (2011) 3890–3896.

[31] J.-B. Vogt, Fatigue properties of high nitrogen steels, J. Mater. Process. Technol. 117 (2001) 364–369.

[32] M.C. Marinelli, R. Strubbia, S. Hereñu, I. Alvarez-Armas, Experimental and numerical analysis of short fatigue cracks in lean duplex stainless steels, Procedia Eng. 74 (2014) 183–186.

[33] R. Richter, W. Tirschler, C. Blochwitz, In-situ scanning electron microscopy of fatigue crack behaviour in ductile materials, Mater. Sci. Eng.: A 313 (2001) 237–243.

[34] O. Düber, B. Künkler, U. Krupp, H. Christ, C. Fritzen, Experimental characterization and two-dimensional simulation of short-crack propagation in An austenitic–ferrita duplex steel, Int. J. Fatigue 28 (2006) 983–992.

[35] T. Zhai, A.J. Wilkinson, J.W. Martin, A crystallographic mechanism for fatigue crack propagation through grain boundaries, Acta Mater. 48 (2000) 4917–4927.

[36] M.C. Marinelli, A. El Bartali, J.W. Signorelli, P. Evrard, V. Aubin, I. Alvarez-Armas, et al., Activated slip systems and microcrack path in LCF of a duplex stainless steel, Mater. Sci. Eng.: A 509 (2009) 81–88.